Journal of Electroanalytical Chemistry 657 (2011) 135–143

Contents lists available at ScienceDirect

Journal of Electroanalytical Chemistry

journal homepage: www.elsevier.com/locate/jelechem

Electrochemical properties of chitosan–Co_3O_4 nanocomposite films

Aarti Sripathi Bhatt, Denthaje Krishna Bhat *, Mysore Sridhar Santosh

Department of Chemistry, National Institute of Technology Karnataka, Surathkal, Srinivasnagar 575 025, India

ARTICLE INFO

Article history:
Received 12 October 2010
Received in revised form 19 February 2011
Accepted 4 April 2011
Available online 9 April 2011

Keywords:
Chitosan–Co_3O_4 films
Impedance
Dielectric constant
Conductivity
Electric modulus
Activation energy

ABSTRACT

Chitosan–Co_3O_4 composite films have been prepared by solution casting method. The obtained films have been characterised by XRD and FESEM. The electrical properties of the films are examined by impedance spectroscopy in the temperature range 303–343 K. The impedance plot of the films pronounces the role of temperature in charge-transfer resistance of the composite. Frequency as well as temperature dependencies of dielectric constant and dielectric loss exhibit the general trend followed by carrier dominated dielectrics. Electric modulus parameters give an insight on the ionic conductivity and relaxation phenomena of the composite films. The dielectric parameters along with modulus data have been exploited to discuss the conduction mechanism in the material. The minimum activation energy of 3.9 kJ mol^{-1} and maximum room temperature conductivity of 1.94×10^{-2} S cm^{-1} were found for composite film with 8% Co_3O_4 content.

1. Introduction

In the recent years, polymers are generally incorporated with additives to bring out a combined effect of both, the polymer as well as the additives. Among the polymers, modern research overtakes biodegradable polymers when compared to the synthetic ones. Commonly identified as biocomposites, these biodegradable polymers are user friendly and economical. Chitosan is one such polymer having good processibility and bacterial property together with biocompatibility and bioactivity [1–3]. Chitosan is the deacetylated form of chitin, a polysaccharide that can be extracted from the shells of crabs, exoskeletons of shrimp and other arthropods [4]. Chitosan forms stable complexes with oxides in solution [5,6]. This polymer is stable in the potential range commonly used, ensuring a high proton conductivity in chitosan complexes [7]. Because of its several such benefits, chitosan is gaining wide importance in the recent times.

Playing with the electrical properties of polymers by incorporating conducting additives not only enhances the overall property of the composite but also widens their applications. There are several studies on conductivity of polymer complexed with salt such as polyethylene oxide (PEO)-salt complexes [8–11], lithium acetate–chitosan complexes [12] and many more. Nevertheless, in the field of electrochemistry, an efficient additive is required to possess good stability and conductivity. Complex metal oxides with spinel structure are known to be active, inexpensive and thermodynamically stable [13]. Among spinel-type metal oxides, Co_3O_4 is generally the preferred additive as it is known to enhance the electrical conductivity of composites [14,15]. Ideal cobalt oxide shows a p-type semiconducting behaviour. However, in the nanoscale, the large surface to volume ratio and the reduced particle size leads to variation in the electrical behaviour of these particles. Nanocrystalline particles are said to enhance dielectric properties [16,17]. Moreover, studies on the effect of temperature and frequency on the dielectric behaviour provide valuable information on the conduction mechanism in the material [18]. A basic understanding of dielectric properties is therefore, needed by most engineers working in the semiconductor industry. Likewise, high proton conductivity is a major requirement in the field of polymer electrolyte membrane (PEM). A perfluorosonic acid membrane or Nafion® (Du Pont) is widely used as proton conducting electrolyte membrane due to its excellent proton conductivity (1.4×10^{-2} S cm^{-1}). [19]. However utilisation of Nafion® in industries is constrained due to its high cost. Hence the development of more cost-effective membranes with suitable proton conductivity especially at higher temperatures is crucial. Inclusion of lithium salts to polymer membranes is known to enhance conductivity [12]. The addition of CaO to chitosan membrane shows a conductivity value in the order of 10^{-3} S cm^{-1} [20]. In the present work, an attempt has been made to analyse the AC conductivity, dielectric and modulus parameters of chitosan–Co_3O_4 composites as a function of temperature and frequency. A survey on the literature shows that studies on electrochemical behaviour of such nanocomposites are limited and hence, requires significance. Also, it is believed that the inclusion of Co_3O_4 in the chitosan membrane will enhance its conductivity leading to its use in conducting based-polymer electrolytes.

* Corresponding author. Tel.: +91 824 2474000X3202; fax: +91 824 2474033.
E-mail address: denthajekb@gmail.com (D.K. Bhat).

1572-6657/$ - see front matter © 2011 Elsevier B.V. All rights reserved.
doi:10.1016/j.jelechem.2011.04.002

2. Experimental

All chemicals used were of analytical grade and high purity. Medium molecular weight chitosan was obtained from Sigma–Aldrich and was used as received. Deionised water was used throughout the study.

2.1. Preparation of Co_3O_4 nanoparticles

In a typical synthesis, 2 g $Co(NO_3)_2{\cdot}6H_2O$ was dissolved in 10 ml ethylene glycol. To this, 8 g of surfactant trioctyl phosphine oxide (TOPO) was added and the solution was sonicated for 30 min to attain homogeneity. The homogeneous solution was then transferred to a Teflon vessel and subjected to microwave irradiation (QWave 1000, Questron Technologies Corp.) at high power. The Teflon vessel was connected to an exhaust to drain off any vapours produced during the reaction. A violet coloured solution was obtained after 5 min, which was centrifuged and washed with acetone and dried at 333 K. The precursor thus obtained was heated at 313 K for 3 h in air to finally yield the black oxide product.

2.2. Preparation of chitosan–Co_3O_4 composite films

Chitosan was dissolved in 2% acetic acid solution (2% m/v). Cobalt oxide nanoparticles were dispersed in this through ultrasonic irradiation. According to the percentage of additive added, the resulting solutions were labelled as PC, CC1, CC2, CC3 and CC4 for 0%, 2%, 4%, 6% and 8% respectively. Addition of Co_3O_4 higher than 8% leads to a heterogeneous solution. After sonication, the composite blends were solution casted on Teflon plates and dried at 333 K for 24 h. The films formed were further soaked in distilled water for 24 h to remove residual solvent.

2.3. Electrochemical studies

Electrochemical impedance measurements were carried out using an electrochemical work station, AUTOLAB 30. The films were placed in between two square copper electrodes (length 2 cm) fitted with copper wires (Fig. 1). The whole set up was held tightly with a plastic clamp. 1 M KOH solution was used as electrolyte. Electrochemical measurements were carried out using a small amplitude AC signal of 10 mV over a frequency range of 100 kHz–0.01 Hz. Experiments were carried out at room temperature and at higher temperatures (313 K–343 K). An oil bath was used to maintain the required constant temperature. Minimum three readings were taken for each sample.

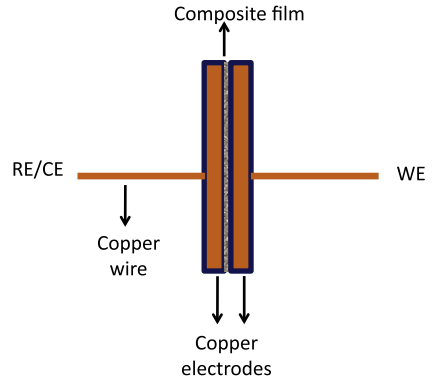

Fig. 1. Cross section of the electrode system (WE, RE and CE represent working electrode, reference electrode and counter electrode respectively).

2.4. Instrumentation

The X-ray powder diffraction analysis for Co_3O_4 nanoparticles was conducted on a JEOL X-ray Diffractometer at a scanning rate of 2° per minute with 2θ ranging from 20° to 80°, using CuK_α radiation (λ = 1.5406 Å). XRD samples were prepared by placing the particles/composite films on a glass slide. Investigations on the morphology and size of Co_3O_4 nanoparticles were carried out using a Transmission Electron Microscope (TEM, JEOL, 2000FXII) operated at 200 kV. TEM specimens were prepared by placing single drops of dilute particle solutions in acetone onto continuous carbon support films and allowing the solvent to evaporate. The instrument is also capable of determining the selected-area electron diffraction pattern.

3. Results and discussion

3.1. Characterisation of Co_3O_4 nanoparticles and chitosan–Co_3O_4 composite films

Fig. 2a shows the bright field TEM images of the cobalt oxide samples. The SAED pattern shown in Fig. 2c has well indexed ring pattern which correspond to CO_3O_4, further supported by XRD results. Sampling about 150 particles from different TEM micrographs showed that they are almost uniform with a standard deviation of less than 13%. From the particle size analysis (Fig. 2b) [21–23] the average diameter D_{TEM} of the particles was found to be 6 nm.

The XRD pattern of the synthesised nanoparticles is shown in Fig. 3. The diffraction peaks can be assigned to a cubic phase of Co_3O_4 according to JCPDS 43-1003, indicating the formation of spinel Co_3O_4. The small peak intensities reveal the nanosize formation of grains. Using the Debye–Scherrer equation, the average crystallite size of the nanoparticles was calculated to be 8 nm, which agrees quite well to that estimated by TEM measurements. The figure also shows the XRD pattern of the composite samples. The prominent peak at 37.89° corresponding to (3 1 1) plane of the spinel Co_3O_4 can be seen in all composite films. This shows the successful incorporation of the nanoparticles into the chitosan polymer matrix.

3.2. Electrochemical impedance spectroscopy measurements

Electrochemical impedance spectroscopy is a well-established powerful technique for investigating many electrical properties of materials and their interfaces. This technique has been mainly used to study corrosion processes, interfacial reaction mechanisms and dynamics of mobile charge in bulk or interfacial regions of any material. Material properties like conductivity, dielectric constant and activation energy can be deduced from EIS data. In all the measurements related to impedance, at least three similar results were considered and their average values are reported.

Fig. 4 shows the room temperature Nyquist plots for the blank polymer film and composite films. The impedance spectra show a semi-circle behaviour corresponding to the charge-transfer process. The diameter of the semi-circle represents the charge-transfer resistance (R_{ct}) at the electrode surface. The impedance spectral data was fitted with the Randles circuit which consists of a parallel capacitance and charge-transfer resistance (R_{ct}) in series with solution resistance (R_s). R_{ct} value depends on the insulating and barrier properties at the electrolyte/electrode interface [24], the values of which are given in Table 1.

In Fig. 4, the Nyquist plot for blank polymer was found to have a large semi-circle domain ($R_{ct} = 2.5275 \times 10^3$ ohms), which implied a very large charge-transfer resistance. However, after the incorpo-

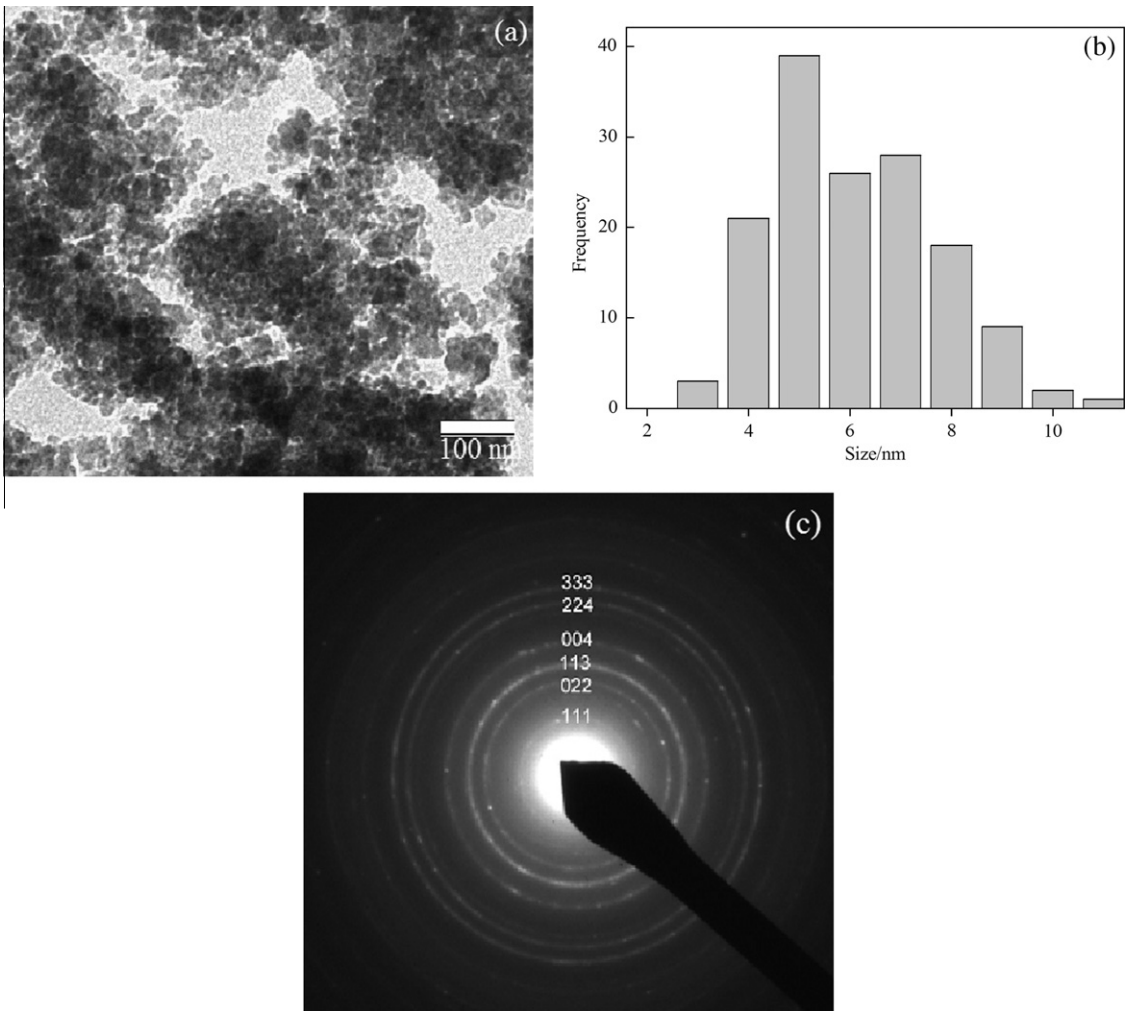

Fig. 2. (a) Bright field TEM image of Co_3O_4 nanoparticles (b) Size distribution histogram of the particles obtained by TEM analysis (c) SAED pattern of Co_3O_4 nanoparticles.

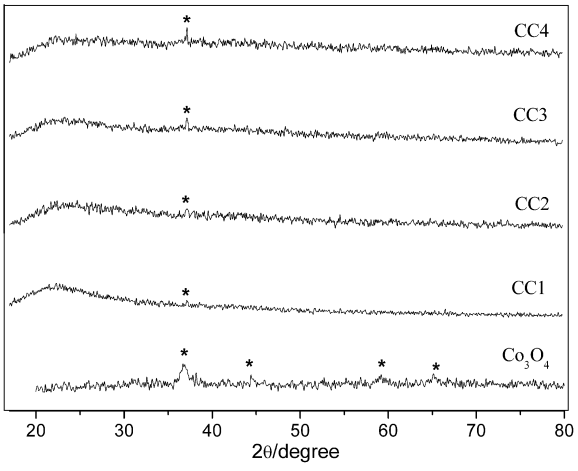

Fig. 3. X-ray diffraction patterns of Co_3O_4 nanoparticles and composite films.

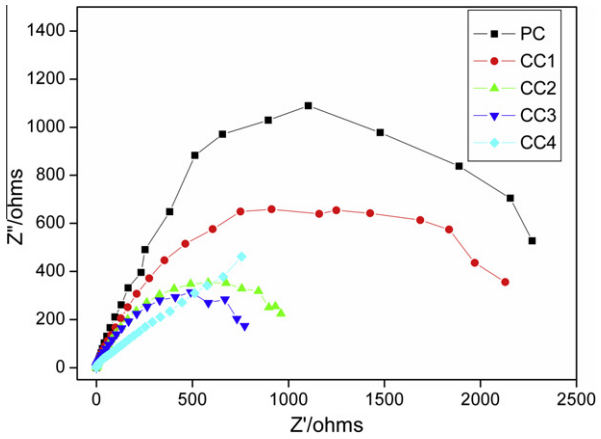

Fig. 4. Room temperature Nyquist plots.

ration of cobalt oxide nanoparticles, the charge-transfer resistance decreased. Among the composite films, along with the increase in the content of nanoparticles, the charge-transfer resistance decreased dramatically. This clearly indicates that cobalt oxide nanoparticles facilitate the charge transfer between the electrolyte and the electrode.

3.3. Effect of temperature

The effect of temperature on the charge-transfer resistance of polymer film and composite films was studied by measuring the impedance at different temperatures from 313 K to 343 K. Fig. 5 shows the Nyquist plots at different temperatures for

Table 1
R_{ct} values (in ohms) for pure and composite films at different temperatures.

	PC	CC1	CC2	CC3	CC4
303 K	2.5275×10^3	1.9287×10^3	1.1182×10^3	8.9231×10^2	9.7484×10^1
313 K	2.5116×10^3	5.8511×10^2	5.2657×10^2	3.6050×10^2	7.4801×10^1
323 K	4.7731×10^2	3.5551×10^2	3.9387×10^2	2.4969×10^2	6.1416×10^1
333 K	2.7802×10^2	2.8834×10^2	3.2594×10^2	1.8648×10^2	5.6011×10^1
343 K	2.4267×10^2	1.8885×10^2	1.0178×10^2	1.7261×10^2	4.7447×10^1

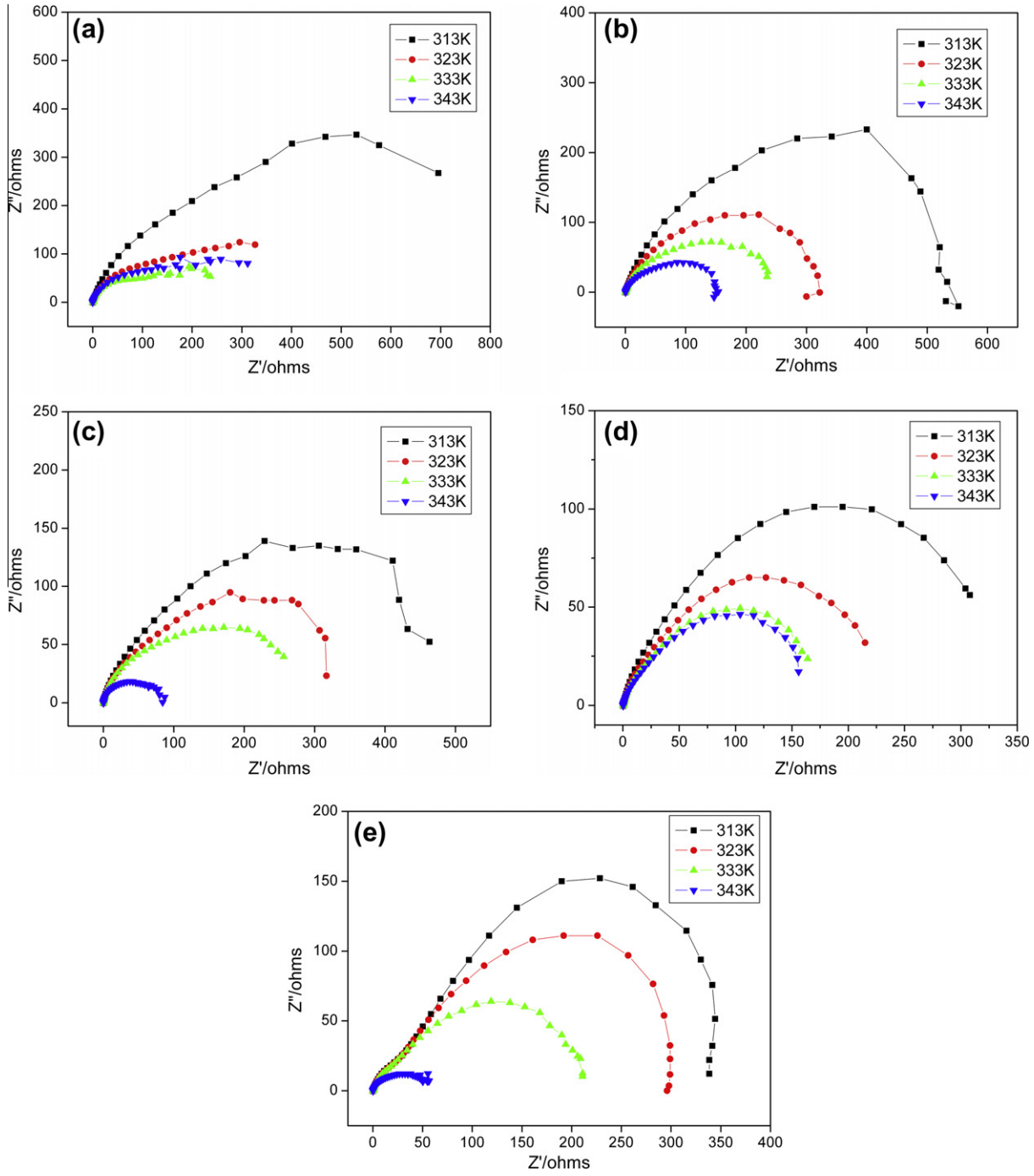

Fig. 5. Nyquist plots for (a) PC (b) CC1 (c) CC2 (d) CC3 (e) CC4 at different temperatures.

the polymer and composite films. It can be clearly observed that an increase in temperature decreased the charge-transfer resistance of all films. The corresponding R_{ct} values are shown in Table 1.

3.4. Dielectric studies

Impedance is a complex number and is represented by a real part Z' and an imaginary part Z'' with the formula

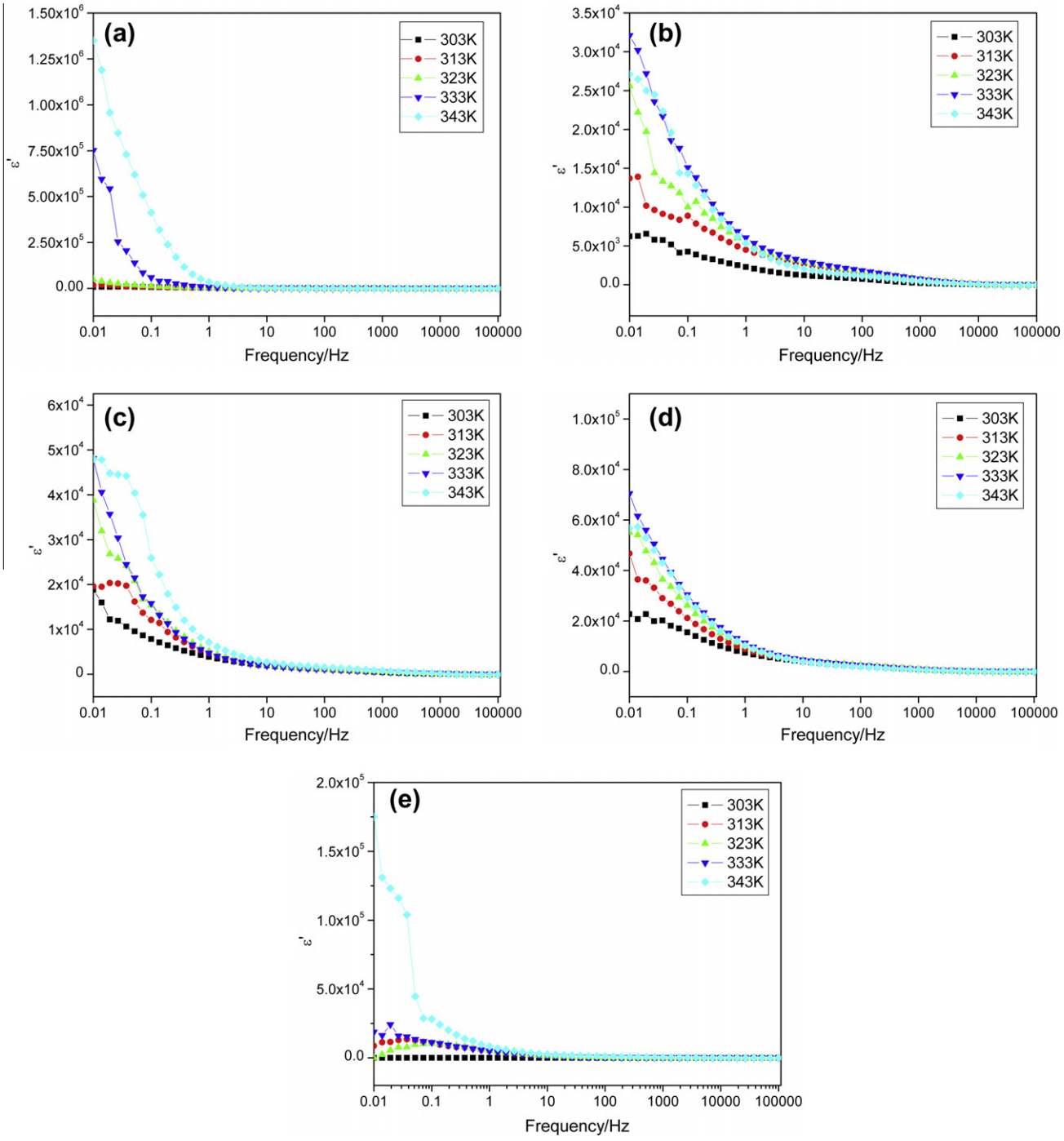

Fig. 6. Frequency variation of ε' of (a) PC (b) CC1 (c) CC2 (d) CC3 and (e) CC4 at different temperatures.

$$Z = Z' + jZ'' \tag{1}$$

where j is $\sqrt{-1}$.

The dielectric constant ε_R, the dielectric loss ε_I, the real electrical modulus M_R and the imaginary electrical modulus M_I can be shown by

$$\varepsilon_R = \frac{Z_I}{\omega C_0 (Z_R^2 + Z_I^2)} \tag{2}$$

$$\varepsilon_I = \frac{Z_R}{\omega C_0 (Z_R^2 + Z_I^2)} \tag{3}$$

$$M_R = \frac{\varepsilon_R}{(\varepsilon_R^2 + \varepsilon_I^2)} \tag{4}$$

$$M_I = \frac{\varepsilon_I}{(\varepsilon_I^2 + \varepsilon_R^2)} \tag{5}$$

Here $C_0 = \frac{\varepsilon_0 A}{t}$ and ε_0 is the permittivity of free space, A is the electrolyte–electrode contact area and t is the thickness of the sample and $\omega = 2\pi f$, f being the frequency in Hz.

The variation of the real and imaginary part of the dielectric constant with frequency of the applied field for temperatures from 303 to 343 K is shown in Figs. 6 and 7. The dielectric properties are

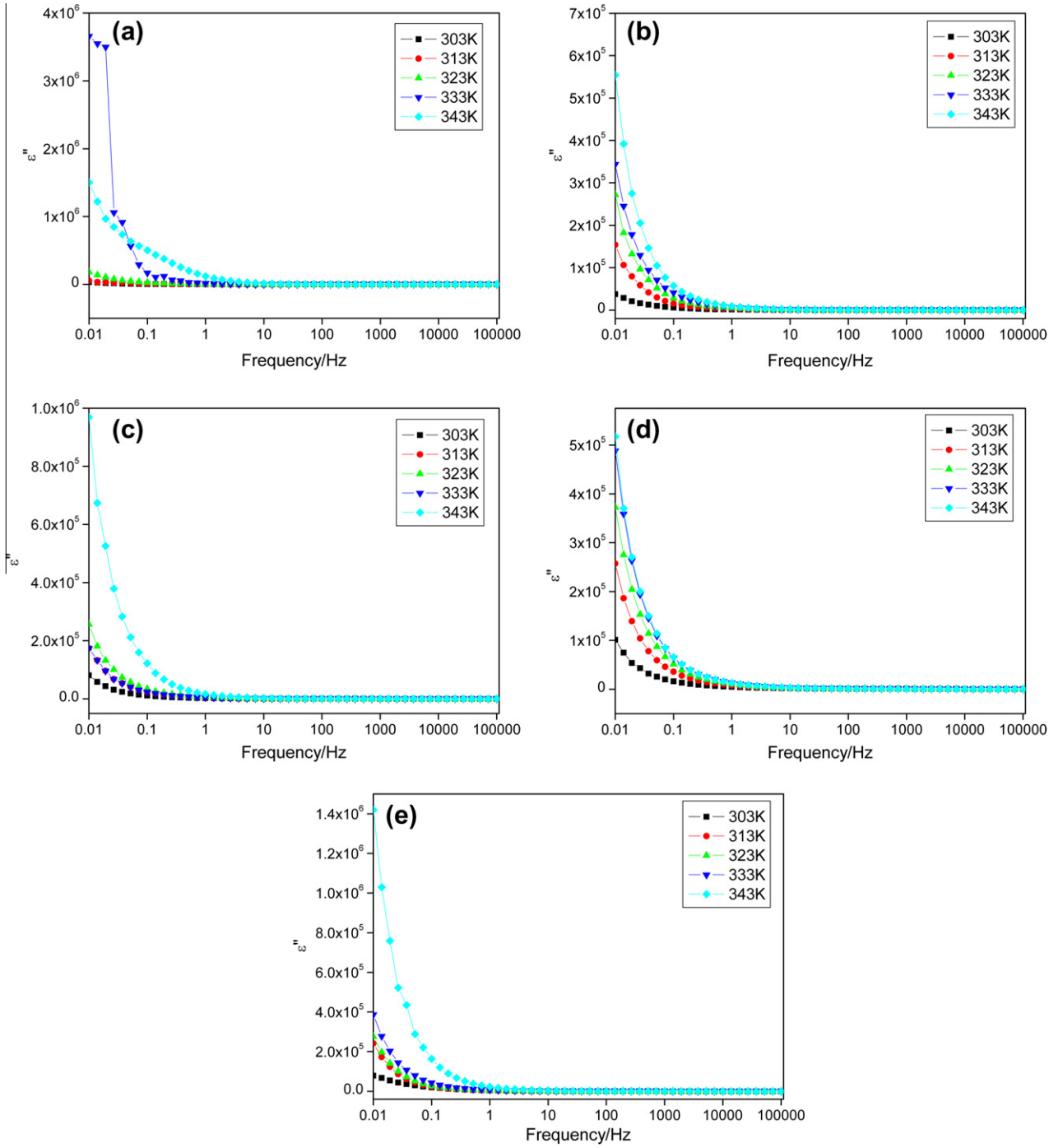

Fig. 7. Dielectric loss as a function of frequency for (a) PC (b) CC1 (c) CC2 (d) CC3 and (e) CC4 at different temperatures.

influenced by several factors like method of preparation, sintering conditions, ionic charge, grain size, etc. It can be seen that ε' decreases with increasing frequency at constant temperature. On the other hand, ε' increases with increasing temperature at constant frequency. A similar trend was seen by Makhlouf [25] for nickel oxide thin films. Fe_3O_4–chitosan composites also followed a similar pattern [26].

The analysis shows a decrease in dielectric constant with increasing frequency and reaches a constant value beyond a certain frequency limit (at higher frequency region) for all samples. Such kind of dispersion is mainly due to the Maxwell–Wagner type of interfacial polarisation and in conformity with the Koop's phenomenological theory [27]. According to theory, the dielectric behaviour of nanostructured materials is primarily due to different types of polarisation present in the material [28]. The variations in dielectric constant can be explained by assuming the mechanism of dielectric polarisation which is similar to hopping conduction mechanism [29]. The polarisation is mainly generated by electron exchange between Co^{2+} and Co^{3+} ions which results in local displacement of charges. Such a kind of electron exchange is commonly observed in ferrites [30,31]. One more factor responsible for the large value of dielectric constant at lower frequency is oxygen vacancies in the interfaces of nanostructured materials. These oxygen vacancies are equivalent to positive charges giving rise to dipole moments.

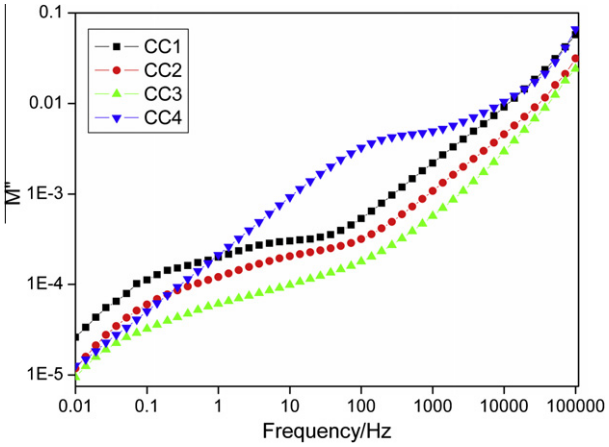

Fig. 8. Concentration dependence of M'' for composite films at 303 K.

When exposed to an electric field, these dipoles rotate, giving a resultant dipole moment in the direction of the applied field. This is called rotation of polarisation direction [32]. Also, the decrease in dielectric constant with frequency is not unusual and may be due to the fact that any species contributing to polarizability lags behind the applied field at higher frequencies [33]. As the temperature increases more and more dipoles orient, resulting in an increase in the dipole moment. Hence, the dielectric constant increases with an increase in temperature. For higher temperature, the values shift upwards.

3.5. Electric modulus studies

From the dielectric studies it was known that ε'' increases with an increase in temperature at low frequency and remains constant at higher frequencies. This behaviour is attributed to conduction mechanism. For a closer inspection of this phenomenon, electric modulus was analysed from the dielectric studies using Eq. (4) and (5)

Macedo introduced electric modulus to study space charge relaxation phenomena [34]. The modulus representation suppresses the signal intensity associated with the electrode polarisation and emphasises small features at higher frequencies. As a result, its usage has been extended to understand the ionic conductivity [35–37]. Electric modulus is basically the reciprocal of permittivity, $M^* = 1/\varepsilon^*$. From the physical point of view, electric modulus corresponds to the relaxation of electric field in the material, where the electric displacement remains constant [38].

Fig. 8 shows the frequency dependence of M'' spectra for different cobalt oxide concentrations at 303 K. It is remarkable that the maximum M'' peak for the sample with highest amount of filler shifts to higher frequency (CC4) compared to other compositions. Only a slight increase in frequency is observed for the other three composite films. The shifting of peaks to higher frequency as the conductivity increases indicates that the relaxation time decreases

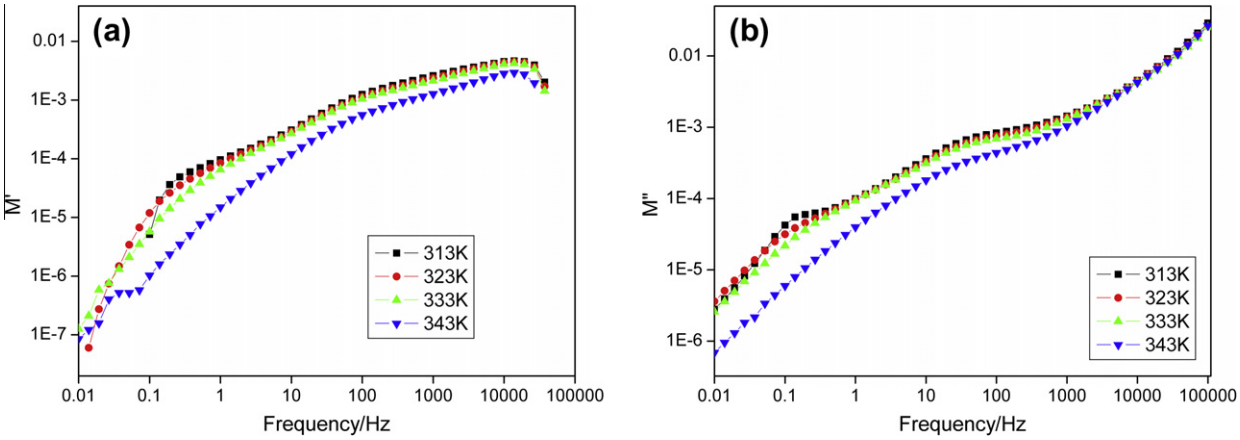

Fig. 9. Frequency dependence of (a) M' and (b) M'' at different temperatures for CC4 film.

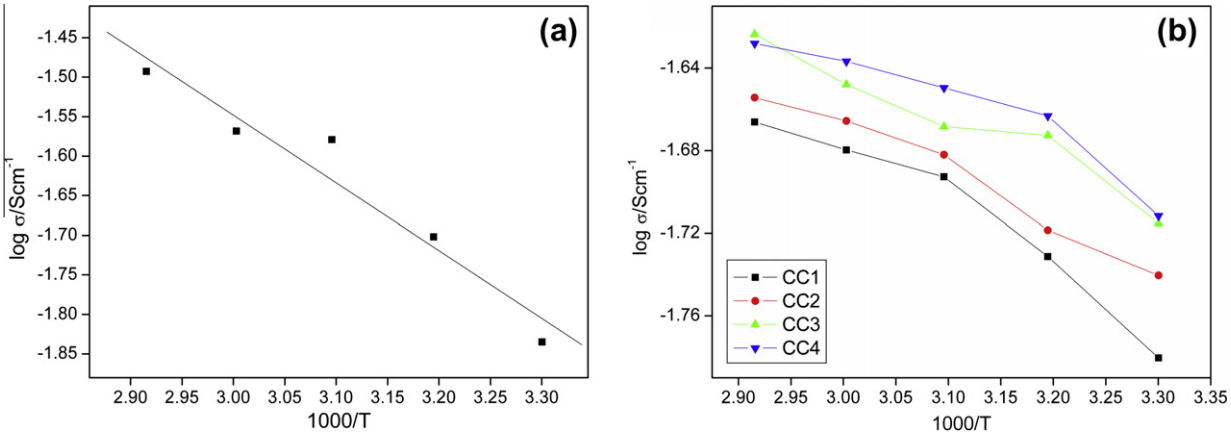

Fig. 10. Arrhenius plots for conductivity σ of (a) chitosan film and (b) composite films.

Table 2
Room temperature conductivity values and activation energies for the polymer films.

Sample	R^2	*Ea* (k Jmol^{-1})	σ (S cm^{-1})
PC	0.941	16.39	1.46×10^{-2}
CC1	0.936	5.63	1.66×10^{-2}
CC2	0.972	4.50	1.82×10^{-2}
CC3	0.945	4.15	1.93×10^{-2}
CC4	0.889	3.90	1.94×10^{-2}

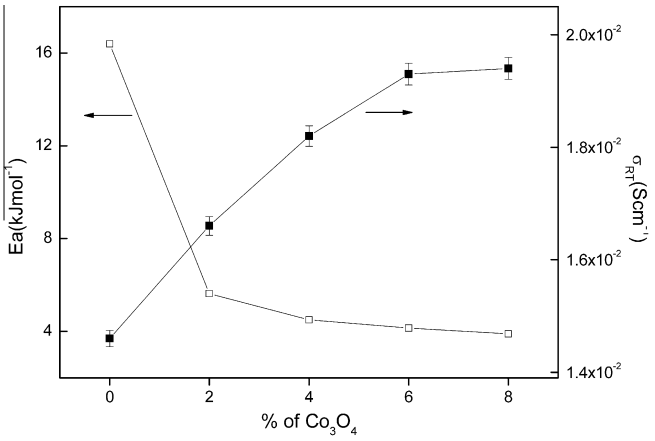

Fig. 11. Variation of activation energy Ea and room temperature conductivity σ_{RT} as a function of Co_3O_4.

as the conductivity increases [39]. Moreover, the broad nature of the peaks suggests a non-Debye type of relaxation in the material [40].

Fig. 9 shows the frequency dependence of the real and imaginary parts of the electric modulus at higher temperatures for the sample with the highest conductivity (CC4). It can be seen from Fig. 9a that M' value increases with an increase in frequency indicating the distribution of relaxation processes over a large range of frequencies [41]. Very small values of M' at lower frequencies is a sign of removal of electrode polarisation [42,43]. A decline in the values of M' with the increase in temperature results from an increase in the mobility of the polymer segment and charge carriers with the temperature. At high temperatures, the orientation of the charge carriers and molecular dipoles become easier.

Comparisons of the ε^* and M^* representations have been used to distinguish localised dielectric relaxations processes from long range conductivity. Generally, for a conduction process, a relaxation peak would be observed in the frequency spectra of the imaginary component M″ and no peak would exist in the corresponding plot of ε″. However, for a dielectric relaxation process, a relaxation peak appears in both ε″ as well as M″ representations [44,45]. The formation of loss peaks in Fig. 9b whereas; absence of such a peak in Fig. 7 ascertains a conduction process for relaxation. Moreover, the peaks are broad and asymmetric; where the low frequency side of the peak represents the range of frequencies in which the ions are capable of moving long distances, i.e. performing successful hopping from one site to the neighbouring site, whereas, for the high frequency side, the ions are spatially confined to their potential wells and can execute only localised motion [46]. This predicts non-Debye behaviour. The appearance of more than one peak at 313 K in the low frequency region may be due to the polar group relaxations. This peak disappears at higher temperatures, which can be ascribed to the high mobility of charge carriers within the material [47]. Also, it is clear from the figure, that irrespective of the temperature at which the measurements were made, all the curves merge at higher frequency. At higher frequencies, the contribution from the grain predominates due to the absence of the space charge effects.

3.6. Conductivity studies

Electrical conductivity of nanoparticles of metals, alloys and semiconductors are reported to be markedly different from their bulk counterparts [48–50]. Semiconductor nanostructures are said to show enhanced conductivity in nanosize regime [51].

The bulk ionic conductivities (σ) of the composite polymer films were determined from the complex impedance spectra using the equation

$$\sigma = \frac{L}{RA} \tag{6}$$

where L, A and R are respectively, the thickness, area and bulk resistance of the polymer films. The bulk resistance was calculated from the high frequency intercept on the real impedance axis of the Nyquist plot [52]. The temperature dependence of conductivity for the pure film and composite films is shown in Fig. 10. It can be seen that conductivity increases with an increase in temperature for all samples. The observed behaviour clearly indicates that the chitosan–Co_3O_4 composite films have a semiconductor-like behaviour. According to Rabkin and Novikova [53], the process of dielectric polarisation in ferrites takes place through a mechanism similar to the conduction process. By electronic exchange, $Co^{2+} \leftrightarrow Co^{3+}$, local displacements of the electrons in the direction of applied field takes place; this results into polarisation. Both n and p type of carriers contribute equally to polarisation and the process is highly temperature dependent. Since the influence of temperature is more pronounced in $Co^{2+} \leftrightarrow Co^{3+}$ electronic exchange than on the displacements of p-carriers, the easy electronic exchange requires less energy thereby increasing the conductivity.

One of the important variables resulting from the electrical properties of semiconductor is its activation energy (*Ea*). This is the initial energy that the charge carriers need to move inside the material. *Ea* is evaluated from the slopes of log σ versus temperature plots, using the following relation

$$\sigma = \sigma_0 \exp[-Ea/kT] \tag{7}$$

where σ is the conductivity at a particular temperature, σ_0 is the pre-exponential factor, k is the Boltzmann's constant and T is the absolute temperature. Fitment of the plots in Fig. 10 gives a straight line with the regression value, R^2 in the range of 0.889–0.972, indicating that the relationship between log σ versus $10^3/T$ is almost linear and hence, follows the Arrhenius rule. In the present work, the activation energy for pure chitosan film is found to be 16.39 kJ mol^{-1} which is in agreement with the reported value [54]. The conductivity values and activation energy for the films are given in Table 2. Fig. 11 shows how the room temperature conductivity and activation energies vary as a function of the filler content. The decrease in Ea with increase in Co_3O_4 content can be explained on the basis of increase in conductivity. Given that conductivity and activation energy are inversely proportional to each other, Eq. (7), such a trend is not unexpected since a high conductivity increases the probability of electron exchange, thereby, decreasing the activation energies [55,56]. This further supports the hopping mechanism of conduction.

4. Conclusion

Chitosan–Co_3O_4 composite films were prepared by solution casting technique. The formation of Co_3O_4 nanoparticles was confirmed by TEM. XRD was used to show the successful incorporation of Co_3O_4 into the chitosan matrix. Electrochemical Impedance Spectroscopy was employed as a successful tool to calculate the

dielectric properties and electric modulus parameters of the samples. The charge transfer values increased with an increase in the content of Co_3O_4 and temperature. High permittivity and dielectric loss were obtained for the composite films at low frequency. The dielectric measurements suggested a conduction mechanism wherein, the conduction is mainly based on electronic exchange between Co^{2+} and Co^{3+} ions. The frequency plots of imaginary components of dielectric constant and modulus suggests the relaxation to be of non-Debye type. Conductivity and activation energies show inverse trends of variation with each other due to their inverse interdependence. The conductivity values of the composite films are in par with the conventional polymer systems and hence, have potential application in the development of electrochemical devices and as conducting based-polymer electrolyte.

Acknowledgments

We thank Dr. Cheuk-wai Tai (Stockholm University, Sweden) for helping out with TEM measurements. Financial assistance in the form of an R&D project grant from DST, Govt. of India is gratefully acknowledged. ASB is thankful to NITK Surathkal for the award of a research Fellowship.

References

[1] S. Deb, J. Giri, S. Dasgupta, D. Datta, D. Bahadur, Bull. Mater. Sci. 26 (2003) 655–660.
[2] Y.-C. Chang, D.-H. Chen, J. Colloid Interface Sci. 283 (2005) 446–451.
[3] D.-S. Jiang, S.-Y. Long, J. Huang, H.-Y. Xiao, J.-Y. Zhou, Biochem. Eng. J. 25 (2005) 15–23.
[4] D.S. dos Santos, A. Bassi, J.J. Rodrigues, L. Misoguti, O.N. Oliveira, C.R. Mendonca, Biomacromolecules 4 (2003) 1502–1505.
[5] J. Guzman, I. Saucedo, R. Navarro, J. Revilla, E. Guibal, Langmuir 18 (2002) 1567–1573.
[6] R. Navarro, J. Guzman, I. Saucedo, J. Revilla, E. Guibal, Macromol. Biosci. 3 (2003) 552–561.
[7] B. Smitha, S. Sridhar, A.A. Khan, Macromolecules 37 (2004) 2233–2239.
[8] P.V. Wright, Br. Polym. J. 7 (1975) 319–325.
[9] M. Alamgir, R.D. Moulton, K.M. Abraham, Electrochim. Acta 36 (1991) 773–782.
[10] R. Frech, S. Chintapalli, Solid State Ionics 85 (1996) 61–66.
[11] L.A. Dominey, V.R. Koch, T.J. Blakley, Electrochim. Acta 37 (1992) 1551–1554.
[12] M.Z.A. Yahya, A.K. Arof, Eur. Polym. J. 38 (2002) 1191–1197.
[13] S. Trasatti, Electrodes of Metallic Oxides, Elsevier, Amsterdam, 1980.
[14] M. Oshitani, H. Yufu, K. Takashima, S. Tsuji, Y. Matsumaru, J. Electrochem. Soc. 136 (1989) 1590–1593.
[15] N.J. Tharayil, S. Sagar, R. Raveendran, A.V. Vaidyan, Phys. B 399 (2007) 1–8.
[16] W. Puin, P. Heitjans, Nanostruc. Mater. 6 (1995) 885–888.
[17] P. Marquardt, Phys. Lett. A 123 (1987) 365–368.
[18] C. Mo, Z. Yuan, L. Zhang, C. Xie, Nanostruct. Mater. 2 (1993) 47–54.
[19] L.V.S. Lopes, D.C. Dragunsk, A. Pawlicka, Electrochim. Acta 48 (2003) 2021–2027.
[20] N.C. Mat, A. Liong, Eng. Lett. 17 (2009) 14–17.
[21] T. He, D. Chen, X. Jiao, Y.XuY. Gu, Langmuir 20 (2004) 8404–8408.
[22] A.C.J. Peck, J. Wang, J.B. Tracy, NANO 3 (2009) 1077–1084.
[23] H. Yang, J. Ouyang, A. Tang, J. Phys. Chem. B 111 (2007) 8006–8013.
[24] L. Yang, W. Wei, J. Xia, H. Tao, P. Yang, Anal. Sci. 21 (2005) 679–684.
[25] S.A. Makhlouf, Thin Solid Films 516 (2008) 3112–3116.
[26] A.S. Bhatt, D.K. Bhat, M.S. Santosh, Phys. B 405 (2010) 2078–2082.
[27] C.G. Koops, Phys. Rev. 83 (1951) 121–124.
[28] C.-M. Mo, L. Zhang, G. Wang, Nanostruct. Mater. 6 (1995) 823–826.
[29] N. Rezlescu, E. Rezlescu, Phys. Status Solidi A 23 (1974) 575–582.
[30] S.C. Watawe, B.D. Sarwade, S.S. Bellad, B.D. Sutar, B.K. Chougule, J. Magn. Magn. Mater. 214 (2000) 55–60.
[31] G. Rangamohan, D. Ravinder, A.V. Ramana Reddy, B.S. Boyanov, Mater. Lett. 40 (1999) 39–45.
[32] J. Maier, S. Prill, B. Reichert, Solid State Ionics 28 (1988) 1465–1469.
[33] B. Ramesh, D. Ravinder, Mater. Lett. 62 (2008) 2043–2046.
[34] P.B. Macedo, C.T. Moynihan, R. Bose, Phys. Chem. Glasses 13 (1972) 171–179.
[35] C.A. Angell, Chem. Rev. 90 (1990) 523–542.
[36] R. Richert, J. Non-Cryst. Solids 305 (2002) 29–39.
[37] M.D. Migahed, M. Ishra, T. Fahmy, A. Barakat, J. Phys. Chem. Solids 65 (2004) 1121–1125.
[38] A. Molak, M. Paluch, S. Pawlus, J. Klimontko, Z. Ujma, I. Gruszka, J. Phys. D: Appl. Phys. 38 (2005) 1450–1460.
[39] M.Z.A. Yahya, A.K. Arof, Carbohydr. Polym. 55 (2004) 95–100.
[40] M. Ram, S. Chakrabarti, J. Alloys Compd. 462 (2008) 214–219.
[41] L.N. Patro, K. Hariharan, Mater. Chem. Phys. 116 (2009) 81–87.
[42] F. Yakuphanoglu, Phys. B 393 (2007) 139–142.
[43] A. Dutta, T.P. Sinha, P. Jena, S. Adak, J. Non-Cryst. solids 354 (2008) 3952–3957.
[44] I.M. Hodge, M.D. Ingram, A.R. West, J. Electroanal. Chem. 74 (1976) 125–143.
[45] R. Gerhardt, J. Phys. Chem. Solids 55 (1994) 1456–1491.
[46] J.S. Kim, J. Phys. Soc. Jpn. 70 (2001) 3129–3133.
[47] S.B. Aziz, Z.H.Z. Abidin, A.K. Arof, Polym. Lett. 4 (2010) 300–310.
[48] K. Frahm, B. Muhlschlegel, R. Nemeth, Phys. B 78 (1990) 91–97.
[49] C. Suryanarayana, Bull. Mater. Sci. 17 (1994) 307–346.
[50] Y.-M. Chiang, E.B. Lavik, D.A. Blom, Nanostruct. Mater. 9 (1997) 633–642.
[51] M. Abdulkhadar, B. Thomas, Nanostruct. Mater. 10 (1998) 593–600.
[52] N.A. Choudhury, A.K. Shukla, S. Sampath, S. Pitchumani, J. Electrochem. Soc. 153 (2006) A614–A620.
[53] L.I. Rabkin, Z.I. Novikova, Izs. Acad. Nauk. BSSR, Minsk. (1960) 146.
[54] W. Wang, D. Xu, Int. J. Biol. Macromol. 16 (1994) 149–152.
[55] V.R.K. Murthy, S. Shobhoanadri, Phys. Status Solidi A 38 (1976) 647–651.
[56] M.A. Ahmed, M.A. El Hiti, M.K. El Nimr, M.A. Amer, J. Magn. Magn. Mater. 152 (1996) 391–395.